García-Collado, A., Romero-Carrillo, P. E., Dorado-Vicente, R., & Gupta, M. K. (2023). Studying the effect of short carbon fiber on fused filament fabrication parts roughness via machine learning. 3D Printing and Additive Manufacturing, 10(6), 1336-1346.
Final publication is available from Mary Ann Liebert, Inc.: http://dx.doi.org10.1089/3dp.2021.0304

Studying the Effect of Short Carbon Fiber on Fused Filament Fabrication Parts Roughness via Machine Learning

A. García-Collado[1], P. Romero-Carrillo[2], R. Dorado-Vicente[1]*, M. K. Gupta[3]

[1]Department of Mechanical & Mining Engineering, University of Jaén, 23071, Jaén, Spain

[2]Depart. of Mechanics, University of Córdoba, Edificio Paraninfo, 14071, Córdoba, Spain

[3]Faculty of Mechanical Engineering, Opole University of Technology, 76 Proszkowska St., 45-758 Opole, Poland, Email: munishguptanit@gmail.com, https://orcid.org/0000-0002-0777-1559

*Corresponding author. E-mail address: rdorado@ujaen.es; Tel.: +34 953-212439

Abstract: Along with the characteristic staircase effect, short carbon fibers, added to reinforce Fused Filament Fabrication parts, can significantly worsen the resulting surface finishing. Concerning this topic, the present work intends to improve the existing knowledge by analysing 2400 measurements of arithmetic mean roughness R_a corresponding to different combinations of six process parameters: the content by weight of short carbon fibers in PETG filaments *f*, layer height *h*, surface build angle θ, number of walls *w*, printing speed *s*, and extruder diameter *d*. The collected measurements were represented by dispersion and main effect plots. These representations indicate that the most critical parameters are θ, *f*, and *h*. Besides, up to a carbon fiber content of 12%, roughness is mainly affected by the staircase effect. Hence, it would be likely to obtain reinforced parts with similar roughness to unreinforced ones. Different machine learning methods were also tested to extract more information. The prediction model of R_a using the Random Forest algorithm showed a correlation coefficient equal to 0.94 and a mean absolute error equal to 2.026 µm. On the other hand, the J48 algorithm identified a combination of parameters (h = 0.1 mm, d = 0.6 mm, and s = 30 mm/s) that, independently of the build angle, provides a R_a < 25 µm when using a 20% carbon fiber PETG filament. An example part was printed and measured to check the models. As a result, the J48 algorithm correctly classified surfaces with low roughness (R_a < 25 µm), and the Random Forest algorithm predicted the R_a value with an average relative error of less than 8 %.

Keywords: FFF, Short Carbon Fiber, Machine Learning, Mean Roughness, Random Forest, Decision Tree.

1. Introduction

Additive manufacturing (AM), developed to reduce the tooling investment required to obtain parts with complex geometries, is currently a driven technology of industry 4.0 [1] and can provide from small to large production runs. AM helps to produce parts, layer by layer, usually in a single machine (3D printer), from a previously created digital model. Through this approach, AM can contribute to flexible and rapid manufacturing by reducing tooling, operations, and the number of parts and providing products with complex shapes. Nevertheless, AM technologies still have some challenges, mainly in the slicing, shape optimization, or pre-and-post-processing stages [2]. Different additive manufacturing technologies are available, although the most widespread is Fused Filament Fabrication or FFF, also called Fused Deposition Modelling or FDM. This technology is based on the fusion and extrusion of a filament made from a thermoplastic material.

1.1. Reinforcement filaments & surface finishing in Fused Filament Fabrication

One of the main handicaps of the FFF technique is the surface quality of the printed parts [3]. Current studies highlight two reasons for the lack of smooth finishing: (i) the effect of tessellation of the original CAD model [4]; (ii) the staircase effect [5]. There are several ways to improve the surface quality of FFF printed parts: post-processing methods such as mechanical polishing (for example, tumbling or sandblasting), machining, vapour smoothing, metalizing, and coating [6], and the optimization of printing process parameters [7]. An increasing number of studies focus on selecting the critical FFF process parameters and discussing their effects on the outputs, such as mechanical properties of the printed parts, quality, and surface roughness [8-13]. Thus, process parameters optimization seems to be an adequate strategy for improving the surface quality of FFF parts.

One of the FFF advantages is the extensive catalogue of materials available in the market. The most used polymers are [14]: polylactic acid (PLA), acrylonitrile butadiene styrene (ABS), polyether ether ketone (PEEK), and polyethylene terephthalate glycol (PETG). Regarding the interaction of process parameters and filament material, Boscheto, Giordano, and Veniali [15] or Vahabli and Rahmati [16] studied the relationship between layer height, build angle, and surface roughness for common materials (without reinforcement) such as ABS, ABS Plus, Polycarbonate, ULTEM 9085.

The above paragraph shows studies about the influence of filament material on surface quality. Nevertheless, few works analyse the relation between surface roughness and the use of filaments reinforced with short carbon fiber (SCF). The addition of short carbon fibers to a polymer matrix improves the mechanical properties of printed parts [17-20]. It also increases the tensile modulus up to 2.2 times, employing fibers with an average length between 60-250 μm in traction specimens [21]. However, the surface quality of printed parts reinforced with carbon fiber is not well understood.

1.2. Surface roughness classification and prediction via machine learning

In recent years, Machine Learning (ML) has become a tool to reduce process variability and increase product quality. The ML capabilities to face AM challenges include design decision support, process and yield optimization, in-situ monitoring, and printing process control [22]. In addition, it is worth mentioning the use of ML techniques to predict the properties of printed parts [23]. Machine learning techniques can be supervised or unsupervised [24]. In supervised learning, each instance or vector of input data is labelled to an output value. In unsupervised learning, each instance is not associated with output. Supervised learning techniques can work with continuous output parameters (surface roughness, tensile strength, printing time, cost) or with categories (good part or bad part). Thus, supervised learning techniques are divided into regression or classification techniques. One of the most widely used ML algorithms is neural networks (NN). An NN has a high evaluation capability to represent complex and highly non-linear relationships between input and output features. There are different neural networks types, although one of the most widely used is the multilayer perceptron [25]. Several research works use the multilayer perceptron (MLP) algorithm to generate models to predict tensile strength, compressive strength, dynamic modulus of elasticity in printed parts using FFF [26].

NNs are complex and do not have graphical output. Therefore, some authors propose the use of other ML algorithms that are easier to explain, such as decision trees [27] or the support vector machine (SVM) [28]. Decision trees are supervised algorithms capable of classifying instances (rough, not very rough) based on the values acquired by the most influential variables [29]. The SVM (a supervised algorithm) allows grouping instances into two sets (good, bad) using an intermediate hyperplane [30].

In the authors' opinion, the current lack of knowledge regarding the effect of fiber content in surface roughness deserves further study. Moreover, it is interesting to test several successful ML solutions, different from the overused NN approach. To face the above issue, this work analyses the arithmetic mean roughness of 48 PETG samples, each one with ten surface build angles, printed using different combinations of fiber content, layer height, extruder diameter, number of walls, and printing speed.

Among the ML algorithms tested in this study, decision-tree and Random Forest help to determine the main printing parameters and capture the relationships among inputs and outputs. They also provide the optimal parameters combination for printing parts with carbon fiber reinforcement. While Section 2.1 describes the samples printed on carbon fiber PETG and the tested factors. Section 2.2 analyses ML solutions to identify the most significant parameters responsible for the surface finishing and explain how to obtain roughness predictions. Section 3 shows the experimental measurements using plots and presents and discusses the ML results that point out that carbon fiber worsens the surface finishing. Moreover, an example of a part printed using a specific combination of parameters is used to validate the proposed predictions. Finally, the main conclusions are drawn in Section 4.

2. Materials and methods

2.1. Experimental procedure

2.1.1. Materials and printing process

In order to assess the influence of short carbon fibers in PETG, three filaments, with differences around 10% in fiber content, were purchased from different manufacturers: (1) PETG polymer filament (2) PETG 12 polymer filament reinforced with around 12% short carbon fibers. (3) PETG 20 polymer filament reinforced with around 20% short carbon fibers. Filament manufacturers provide the carbon content percentage by weight. The material has a diameter of 2.85 mm with variability of ±0.03 mm in diameter. Table 1 summarizes the filaments' mechanical properties. Regarding the default printer parameters, all samples were printed with a 30% infill density, a grid infill pattern, and extrusion and bed temperatures of 235 °C and 70 °C, respectively.

Many printing parameters can influence surface roughness [31,32]. However, to perform a practical study (cost and time-limited), this work only considers the following

parameters: *f* the fiber content by weight, *h* the layer height, θ the surface build angle, *w* the number of outer walls, *d* the nozzle diameter and *s* the printing speed.

2.1.2. Design of experiments to build ML models

A 3D printer Ultimaker® S5 with Ultimaker CURA 4.3 software was used to print samples. Figure 1 shows the printing samples to measure surface roughness. Based on the work of Kim & Oh [33], samples shapes have dimensions of 50 x 30 mm, a height of 27 mm, and ten different build angles from 0° to 90°. The extrusion length is developed in the X-Y plane, and the build-direction is developed in Z.

Table 2 shows the full factorial design with the factors and levels tested. The 48 printed samples help to achieve all combinations. Each sample has 10 build angles (from 0 °C to 90 °C), and in each angle, the arithmetic mean roughness R_a was measured 5 times (2400 measurements). R_a is the arithmetic mean of the absolute values of the profile height deviations from the mean line, recorded within the evaluation length [34]. A commercial Mitutoyo Surftest SJ-210 (Mitutoyo, Kawasaki, Japan) profilometer with a sampling length of 2.5 mm and measuring the speed of 0.5 mm/s provided the R_a measurements. The outcome or response considered to train the machine learning methods was the average R_a of the 5 replications for each angle.

2.2. Machine learning modelling

This section describes the proposed Machine Learning (ML) algorithms to identify the most significant parameters and provide an adequate process parameter configuration. Attached to the ML study, this work includes a visual analysis of the measured data and an approximation model to estimate R_a from the most significant printing factors.

2.2.1. Data visualization and approximation Model

Data visualization can help identify the most significant factors and their robustness: the observed measurement dispersion. Main effects plots can provide, for each parameter, the system means or dispersion values at its different levels [35]. Besides identifying the main factors, it is possible to determine the most adequate and robust configuration to get low roughness and better mechanical properties. The idea is to identify the best fiber content in the main effect plots regarding the roughness. Finally, for each layer height tested, it is possible to build an *m* x *n* degree polynomial Bézier

patch to estimate R_a as a function of two scaled experimental parameters. The Bézier representation is used for modeling curves and surfaces in CAD programs [36]:

$$R_a = \sum_{i=0}^{m} \sum_{j=0}^{n} b_{ij} B_i^m(u) B_j^n(v) \ , 0 \leq u, v \leq 1. \quad (1)$$

where b_{ij} are the surface control points, and $B_i^m(u), B_j^n(v)$ are the Bernstein polynomials.

The above surface can be fitted to experimental data via least squares. The surface's degree is determined among the lowest values that provide a correlation $r > 0.9$. Although this model establishes a non-linear relationship among the independent and the dependent variable, a linear system is solved to obtain the control points. Because of that, this polynomial regression can be considered a particular case of Multiple Linear Regression (MLR).

2.2.2. Machine learning

Two types of algorithms have been used in this work: classification algorithms and regression algorithms. Classification algorithms generate models capable of predicting the class or category to which an instance belongs from its data or input variables. On the other hand, regression algorithms generate models capable of predicting the numerical values of the output variable from the data corresponding to the input variables. For classification methods, the goal (based on ISO 1302) is to distinguish two groups depending on the roughness of the samples: class 1, for values below 25 μm; class 2, for values above 25 μm. In this type of problem, the following metrics provide the performance of the model: percentage of correctly classified instances; percentage of incorrectly classified instances; kappa statistic. This last parameter measures the concordance between predicted and observed categorizations of a dataset. Values around unity indicate a stronger concordance. For the regression methods, the performance of the model is measured using the following indicators: *r* the correlation coefficient; MAE the Mean Absolute Error; RMSE the Root Mean Squared Error.

A set of well-known ML approaches were trained and tested using the experimental data to determine the best classification and regression algorithms. Table 3 shows the ML classification and regression algorithms assessed in this work. The Waikato Environment for Knowledge Analysis (WEKA) tool [24] was used to implement the ML algorithms and extract knowledge from the experimental dataset. WEKA is one of the

most widely used machine learning software, and it is a frequently applied tool in the manufacturing sector [29,37-41]. WEKA also incorporates attribute selection algorithms, which allow us to know which variables have the greatest influence on the output variable. Usually, when these variables are ignored, the generated models are of higher quality 24. In this work, the Ranker algorithm has been used in the classification and regression problem.

3. Results and discussion

The visual observation of the samples' surfaces helps understand the effect of process parameters on the roughness. Note the surface shape of twelve different samples portrayed in Figure 2 and obtained using a confocal laser microscope LEICA® TCS SP5II. As expected due to the staircase effect, it is possible to consider parallel rows of peaks and valleys in all samples. That supports the idea that a conventional profilometer is enough to characterize the samples' surface finishing. On the other hand, the surface presents a pattern highly dependent on f, h, and θ. The staircase pattern depends on h and θ, while f influences the final height from peak to valley. Figure 2 reveals a high dependency of the surface quality with carbon fiber content, which adds a salt-and-pepper noise on the staircase pattern. Other authors have noted that using filaments reinforced with fibers worsens the surface roughness. For example, García et al. [42] observed higher R_a values on specimens printed using PLA with Graphene nanoplatelets than on specimens printed using PLA, and Wang et al. [20] reported the same phenomenon for carbon fiber reinforced PEEK filaments.

The above phenomenon appears during the extrusion and deposition processes. The extrusion through the nozzle aligns the fiber in the flow direction [43], and the high shear rates at the end of the nozzle promote compression among fibers. Hence, the subsequent expansion out of the nozzle stimulates carbon fibers on the sample's surface, increasing the roughness.

Figure 3 shows the increment in surface noise due to the addition of carbon fiber in the PETG. The absence of carbon fiber (Figure 3. a) generates a surface without noise, where the staircase pattern is the main effect. In contrast, Figures 3 b and c show that the carbon fibers on the surface generate local irregularities in the staircase pattern worsen the surface finishing.

Regarding the experimental measurements, Figure 4 shows the arithmetic mean roughness R_a on each build angle of the printed samples taking into account the percentage of fiber and layer height. From these results, it follows that:

- The fiber content increases R_a values and their dispersion. The values measured on parts manufactured using PETG and PETG 12 showed a lower dispersion than those obtained for PETG 20. While for PETG and PETG 12, the surface quality mainly depends on the staircase pattern, for PETG 20, the irregularities due to the fibers are the dominant effect. This fact explains observed variations and can be seen in Figure 3, where the staircase pattern, although blurred, can be appreciated on the PETG 12 sample but not on the PETG 20 one.
- Regarding the angle, the roughness values seem to draw a convex curve with minimum values at 0° and 90° build angles. The results for PETG and PETG 12 filaments (Figure 3 and 4) agree with the claim of Boschetto et al. [15] or Vahabli & Rahmati [16], who showed how the staircase effect causes the roughness to reach a maximum when parts are printed at angles of around 20°. On the other hand, it was not easy to identify that effect for the PETG 20 filament.
- PETG and PETG 12 lead to similar R_a distributions. Thus parts based on PETG 12 could have similar roughness but better mechanical properties than PETG ones.
- Although samples obtained from PETG 20 filaments have, in general, higher R_a, the presented measurements prove that some specific 3D printer settings led to PETG 20 samples with a R_a similar to that obtained with PETG filaments.
- The maximum roughness obtained for specimens with PETG 20 is similar in both cases represented in Figure 4 (h = 0.1 mm and h = 0.2 mm) and is close to 45 μm. Specimens with PETG and PETG 12 reach maximum values of 25 μm (when using h = 0.1 mm) and 35 μm (when using h = 0.2 mm).

3.1. Main effect and regression model

Representing the experimental data by main effect plots helps compare the process parameters' effect on R_a. Figure 5, made with the scientific software Mathematica®, collects the main effects: R_a mean values with error bars (symmetric to 2 times the standard error of the mean) for the factors and levels detailed in Table 2. Factors that show a larger difference between the maximum and minimum values of mean R_a, such as f, h, and θ, have a higher effect on R_a than factors that show a slight difference, such

as the number of walls and the extruder speed and diameter. For the case of *f*, the roughness shows a constant value and low dispersion up to PETG 12, and θ presents the highest dispersion values. Due to its high dispersion and dependency on the part geometry, θ is not a suitable parameter to control the roughness during the process. However, the other factors show lower dispersion than θ and can be controlled to provide robust responses from the printing system. According to the main factor *f* and considering the coverage factor of 2 used for the error bars, to obtain a $R_a < 25$ μm with a reinforced filament, PETG 12 is the best option since it will provide 18.5 μm < R_a < 21.0 μm with 95% confidence.

While main effect plots allow comparing the importance among factors, the Analysis of Variance (ANOVA) helps quantify the likely importance of each factor. It is possible to compute the ANOVA table (Table 4) assuming responses with equal variances, independent errors, and a normal distribution. This statistical analysis shows that θ, *f*, and *h* p-values provide the strongest evidence for rejecting the null hypothesis (probabilities of F-ratio ~ 1 lower than 0.001). Therefore, they are considered the more significant parameters. The lower the p-value of a factor, the more likely it influences R_a. According to this criterion, the factors studied can be ordered as follows: θ, *f*, *h*, *v*, *d*, and *w*.

For each *h*, and the most important factors: *f* and θ, it is possible to fit the R_a measurements by a polynomial surface that provides roughness estimations. The approximation surfaces were made in the Mathematica® software. Figure 6 shows the resulting degree 2x4 Bézier patches. For both approximations: MAE ≤ 2.34 μm, RMSE ≤ 3.75 μm and $r > 0.90$.

3.2. Machine learning approach

ML classification and regression methods can help better understand the studied factors' effect on R_a. The proposed classification and regression ML models are based on five parameters: *m*, *h*, θ, *d*, and *s*. The Ranker attribute selection algorithm indicates that the variable *w* has the least influence on surface roughness.

3.2.1. Classification algorithms

First, it was necessary to convert the numerical output variable into a categorical one: roughness values below 25 μm were classified in class 1; roughness values above 25 μm were assigned to class 2. The classifier efficiency of different ML algorithms,

measured using the Kappa statistic and the number of correctly and incorrectly classified data, is shown in Table 5. The most successful algorithms are the Random Forest (kappa = 0.8873), the J48 (kappa = 0.8784), and LMT (kappa = 0.8784) algorithms. The Random Forest can correctly classify 95.11 % of the instances (in 10-fold cross-validation). These results are better than those obtained by the algorithm in previous research works for materials without reinforcement [39]. This work uses the J48's results due to its capability to portray the information with a graphic decision tree.

Figure 7 shows the decision tree generated by the J48 algorithm (C4.5), as can be seen:

- Layer height, fiber content, and angle are the most important parameters as they are nodes of the main tree branches.
- Parts printed with PETG 12 and h = 0.1 mm present a surface roughness lower than 25 μm, independently of the value of the build angle. This conclusion substantiates the observations provided by the main effect plots.
- Parts printed with PETG 20 present a surface roughness lower than 25 μm independently of the angle to be printed if the following printing parameters are used: h = 0.1 mm, d = 0.6 mm, and s = 30 mm/s.
- The last observation provides new information that was not attained with the data visualization and the main effect plots. Hence, the authors consider it to be one of the main contributions of the work.

3.2.2. Regression algorithms

It is also possible to define a prediction model based on ML algorithms. Table 6 summarises the regression's MAE, RMSE, and the correlation coefficients for the several ML algorithms tested. The best regression algorithm is Random Forest (r = 0.94). The Random Forest algorithm is one of the preferred ensemble classification algorithms in manufacturing studies. It has been previously used in the literature in the field of additive manufacturing. For example, Wu, Wei, and Terpenny [44] employed it to predict surface roughness on printed parts from data measured using different sensors (table temperature, extruder temperature, table vibration, extruder vibration, melt pool temperature). Figure 8 shows a plot of actual versus predicted values. As shown in the figure, the model generated by the algorithm achieves a good fit for the values corresponding to filament with PETG and PETG 12. In the case of the PETG 20 filament,

the modelling is acceptable in the range of 0 - 25 μm. Above that value, the model finds it more difficult to predict the roughness to be obtained.

3.3. A real example

Printing a part allows checking the goodness of the proposed classification and regression models. The piece printed was the fixture shown in Figure 9 with a configuration that, according to the ML approach used, provides class 1 results, R_a < 25 μm: PTEG20, h = 0.1 mm, d = 0.6 mm and s = 30 mm/s. Ultimaker Cura default definition is maintained for other printer parameters.

Figure 9 portrays the prediction model estimations (Bézier patches and ML regressions) and the actual measurements for different parts' build angles. ML regression identified the expected class 1 roughness (R_a < 25 μm for the defined parameter combination). On the other hand, the polynomial regression failed to predict the class 1 roughness. Finally, we consider that the residuals between experimental values and estimations are acceptable due to the mean relative error lower than 8%.

4. Conclusions

The visual and ML analysis conducted in this work shows that fiber content has an important influence on the R_a measurements on PTEG FFF printed samples. Samples were printed and measured to demonstrate the previous claim: 48 parts, with 10 different build angles (480 measurements in total). The variables studied were: carbon fiber percentage by weight, nozzle diameter, layer height, build angle, printing speed, and the number of perimeters. These are the most relevant results obtained:

- Pictures of a confocal laser microscope show that the staircase pattern mainly depends on layer height and build angle. For those samples printed with PETG 12 and 20, irregularities are noted on the staircase pattern. During extrusion, carbon fibers are compressed, and the subsequent expansion out of the nozzle could explain the presence of fibers on the samples' surfaces and, therefore, the observed irregularities.
- A preliminary analysis of the experimental measures indicates that PETG 12 samples have a surface roughness similar to PETG ones. The maximum R_a for PETG 12 is 25 μm for an h = 0.1 mm and 35 μm for an h = 0.2 mm. $R_a(\theta)$ curve has a shape caused by the staircase effect similar to a normal distribution skewed to the right, already identified previously by other authors. The parts

printed on PETG 20 present higher surface roughness values, reaching maximum values close to 50 μm. On the other hand, the values measured in this case have larger variability and do not seem to follow the $R_a(\theta)$ shape mentioned above, most likely due to the short fibers increasing the noise on the staircase pattern.

- Simple observation of main effect plots and the ANOVA test support that f, θ, and h are the most critical parameters. ML methods also substantiated this claim. Furthermore, a polynomial approximations $R_a(f, \theta)$ for different h provide acceptable roughness predictions: MAE ≤ 2.34 μm, RMSE ≤ 3.75 μm, and $r > 0.90$.

Taking advantage of ML to deal with large datasets and many independent variables, we studied the capabilities of some of these algorithms to classify and model our experimental dataset:

- In the case of the classification problem, the best algorithms are Random forest and J48. Due to J48 can provide a decision tree graphic and has similar efficiency to Random Forest, its classification capabilities allow identifying those parameters combinations that lead to $R_a < 25$ μm. It is worth mentioning that the decision tree provided a combination of parameters (h = 0.1 mm, d = 0.6 mm, and s = 30 mm/s) for 20% fiber content filaments, with a high probability to generate $R_a < 25$ μm, independently of the part build angle. This fact was not observed from the mean effect plots, where PETG 20 is related with an average $R_a > 25$ μm.
- For the regression problem, the model that achieves the best predictions is the Random Forest with MAE = 2.026 μm, RMSE = 3.41 μm and r = 0.94.
- Finally, the J48 classification algorithm correctly identified the class 1 roughness ($R_a < 25$ μm) in the example part used with validation porpoises. On the other hand, the Random Forest regression provided a good prediction with a mean relative error lower than 8%.

Acknowledgements

Grant PID2019-104586RB-I00 funded by MCIN/AEI/10.13039/501100011033, and the Andalusian Economy, Knowledge, Enterprise, and University Council, under grant

HICOOL, reference 1263034, co-financed by the European Regional Development Fund, supported this work.

Author Disclosure Statement

The authors declare that they have no known competing financial interests or personal relationships that could have appeared to influence the work reported in this paper.

References

1. Sartal A, Bellas R, Mejias A, *et al*. The sustainable manufacturing concept, evolution and opportunities within Industry 4.0: A literature review. Advances in Mechanical Engineering. 2020;12(5).
2. Oropallo W, Piegl LA. Ten challenges in 3D printing. Engineering with Computers. 2016;32(1):135-48.
3. Pérez M, García-Collado A, Carou D, *et al*. On Surface quality of engineered parts manufactured by additive manufacturing and postfinishing by machining. 1 ed. Manufacturing HiA, editor2021.
4. Nasr ESA, Al-Ahmari A, Moiduddin K. CAD Issues in Additive Manufacturing. Comprehensive Materials Processing. Oxford: Elsevier; 2014. p. 375 - 99.
5. Pandey P, Reddy N, Dhande S. Slicing procedures in layered manufacturing: a review. Rapid Prototyping Journal. 2003;9(5):274-88.
6. Diegel O, Nordin A, Motte D. In: Springer, editor. A Practical Guide to Design for Additive Manufacturing2019.
7. Perez M, Medina-Sanchez G, Garcia-Collado A, *et al*. Surface Quality Enhancement of Fused Deposition Modeling (FDM) Printed Samples Based on the Selection of Critical Printing Parameters. Materials. 2018;11(8).
8. Adel M, Abdelaal O, Gad A, *et al*. Polishing of fused deposition modeling products by hot air jet: Evaluation of surface roughness. Journal of Materials Processing Technology. 2018;251:73-82.
9. Geng P, Zhao J, Wu W, *et al*. Effects of extrusion speed and printing speed on the 3D printing stability of extruded PEEK filament. Journal of Manufacturing Processes. 2019;37:266-73.
10. Jin Y, Wan Y, Zhang B, *et al*. Modeling of the chemical finishing process for polylactic acid parts in fused deposition modeling and investigation of its tensile properties. Journal of Materials Processing Technology. 2017;240:233-9.
11. Kam M, Ipekci A, Sengul O. Investigation of the effect of FDM process parameters on mechanical properties of 3D printed PA12 samples using Taguchi method. Journal of Thermoplastic Composite Materials. 2021.
12. Plaza E, Lopez P, Torija M, *et al*. Analysis of PLA Geometric Properties Processed by FFF Additive Manufacturing: Effects of Process Parameters and Plate-Extruder Precision Motion. Polymers. 2019;11(10).

13. Popescu D, Zapciu A, Amza C, *et al*. FDM process parameters influence over the mechanical properties of polymer specimens: A review. Polymer Testing. 2018;69:157-66.
14. Ngo T, Kashani A, Imbalzano G, *et al*. Additive manufacturing (3D printing): A review of materials, methods, applications and challenges. Composites Part B-Engineering. 2018;143:172-96.
15. Boschetto A, Giordano V, Veniali F. Surface roughness prediction in fused deposition modelling by neural networks. International Journal of Advanced Manufacturing Technology. 2013;67(9-12):2727-42.
16. Vahabli E, Rahmati S. Improvement of FDM parts' surface quality using optimized neural networks – medical case studies. Rapid Prototyping Journal. 2017;23(4):825-42.
17. Bhandari S, Lopez-Anido RA, Gardner DJ. Enhancing the interlayer tensile strength of 3D printed short carbon fiber reinforced PETG and PLA composites via annealing. Additive Manufacturing. 2019;30.
18. Shanmugam V, Rajendran D, Babu K, *et al*. The mechanical testing and performance analysis of polymer-fibre composites prepared through the additive manufacturing. Polymer Testing. 2021;93.
19. Tekinalp HL, Kunc V, Velez-Garcia GM, *et al*. Higly oriented carbon fiber-polymer composites via additive manufacturing. Composites Science and Technology. 2014;105:6.
20. Wang P, Zou B, Ding S, *et al*. Preparation of short CF/GF reinforced PEEK composite filaments and their comprehensive properties evaluation for FDM-3D printing. Composites Part B-Engineering. 2020;198.
21. Ferreira R, Amatte I, Dutra T, *et al*. Experimental characterization and micrography of 3D printed PLA and PLA reinforced with short carbon fibers. Composites Part B-Engineering. 2017;124:88-100.
22. Jiang J, Xiong Y, Zhang Z, *et al*. Machine learning integrated design for additive manufacturing. Journal of Intelligent Manufacturing. 2020.
23. Meng L, McWilliams B, Jarosinski W, *et al*. Machine Learning in Additive Manufacturing: A Review. Jom. 2020;72(6):2363-77.
24. Witten IH, Frank E, Hall MA, *et al*. Data Mining: Practical Machine Learning Tools and Techniques. 4th Edition ed: Morgan Kaufmann; 2017. CP1-621 p.
25. Qi X, Chen G, Li Y, *et al*. Applying Neural-Network-Based Machine Learning to Additive Manufacturing: Current Applications, Challenges, and Future Perspectives. Engineering. 2019;5(4):721-9.
26. Wang C, Tan X, Tor S, *et al*. Machine learning in additive manufacturing: State-of-the-art and perspectives. Additive Manufacturing. 2020;36.
27. Barrios J, Romero P. Decision Tree Methods for Predicting Surface Roughness in Fused Deposition Modeling Parts. Materials. 2019;12(16).
28. Delli U, Chang S. Automated Process Monitoring in 3D Printing Using Supervised Machine Learning. Procedia Manufacturing. 2018;26:5.

29. Molero E, Fernandez J, Rodriguez-Alabanda O, *et al*. Use of Data Mining Techniques for the Prediction of Surface Roughness of Printed Parts in Polylactic Acid (PLA) by Fused Deposition Modeling (FDM): A Practical Application in Frame Glasses Manufacturing. Polymers. 2020;12(4).
30. Aoyagi K, Wang H, Sudo H, *et al*. Simple method to construct process maps for additive manufacturing using a support vector machine. Additive Manufacturing. 2019;27:353-62.
31. Bikas H, Stavropoulos P, Chryssolouris G. Additive manufacturing methods and modelling approaches: a critical review. International Journal of Advanced Manufacturing Technology. 2016;83(1-4):389-405.
32. Vahabli E, Rahmati S. Application of an RBF neural network for FDM parts' surface roughness prediction for enhancing surface quality. International Journal of Precision Engineering and Manufacturing. 2016;17(12):1589-603.
33. Kim G, Oh Y. A benchmark study on rapid prototyping processes and machines: quantitative comparisons of mechanical properties, accuracy, roughness, speed, and material cost. Proceedings of the Institution of Mechanical Engineers Part B-Journal of Engineering Manufacture. 2008;222(2):201-15.
34. Standard AN. Surface Texture (Surface Roughness, Waviness and Lay). 2009.
35. Jiju A. Design of Experiments for Engineers and Scientists. second edition ed2014.
36. Farin G. Curves and Surfaces for CAGD. 5ª ed2002.
37. Bustillo A, López de Lacalle LN, Fernández-Valdivielso A, *et al*. Data-Mining Modeling for the prediction of wear on forming-taps in the threating of steel components. Journal of Computational Design and Engineering. 2016;3(4):11.
38. Bustillo A, Urbikain G, Perez J, *et al*. Smart optimization of a friction-drilling process based on boosting ensembles. Journal of Manufacturing Systems. 2018;48:108-21.
39. Cerro A, Romero P, Yigit O, *et al*. Use of machine learning algorithms for surface roughness prediction of printed parts in polyvinyl butyral via fused deposition modeling. International Journal of Advanced Manufacturing Technology. 2021;115(7-8):2465-75.
40. Maudes J, Bustillo A, Guerra A, *et al*. Random Forest ensemble prediction of stent dimensions in microfabrication processes. International Journal of Advanced Manufacturing Technology. 2017;91(1-4):879-93.
41. Rodriguez J, Quintana G, Bustillo A, *et al*. A decision-making tool based on decision trees for roughness prediction in face milling. International Journal of Computer Integrated Manufacturing. 2017;30(9):943-57.
42. Garcia E, Nunez PJ, Chacon JM, *et al*. Comparative study of geometric properties of unreinforced PLA and PLA-Graphene composite materials applied to additive manufacturing using FFF technology. Polymer Testing. 2020;91:16.
43. Lewicki J, Rodriguez J, Zhu C, *et al*. 3D-Printing of Meso-structurally Ordered Carbon Fiber/Polymer Composites with Unprecedented Orthotropic Physical Properties. Scientific Reports. 2017;7.

44. Wu D, Wei Y, Terpenny J. Predictive modelling of surface roughness in fused deposition modelling using data fusion. International Journal of Production Research. 2019;57(12):3992-4006.

Tables

Table 1. Mechanical properties of printing filaments used.

Mechanical Properties	PETG	PETG 12	PETG 20
Carbon fiber by weight (%)	0	11.6	20.5
Tensile Modulus (MPa)	3510	4540	5230
Tensile Strength (MPa)	53	52.9	56
Flexural modulus(MPa)	2404	2648	5740
Flexural Strength(MPa)	98.4	80.4	80

Table 2. Design of experiments: factors and levels.

Factor	Symbol	Unit	Levels
Layer height	h	mm	0.1, 0.2
Surface build angle	θ	°	0-90
Material	f	Carbon fiber % (by weight)	PETG, PETG 12, PETG 20
Number of outer walls	w	-	1, 3
Nozzle diameter	d	mm	0.6, 0.8
Printing speed	s	mm/s	30, 60

Table 3. Brief description of classification and regression ML algorithms (Elaborated from Weka Documentation)

Classification	Regression	Classification & Regression
Naive Bayes. Probabilistic classifier		
Logistic. Multinomial logistic regression model with a ridge estimator	*Linear Regression*	*MLP.* Multilayer Perceptron neural network
SMO. Sequential Minimal Optimization	*SMOreg.* Support vector machine for regression	*IBK.* Instance-based learner with parameter k
LibVSM. SMO algorithm for kernelized support vector machines	*M5P.* Decision tree with linear regressions at the leaves.	*K**. Instance-based classifier.
J48 (C4.5). Decision tree algorithm		*Random forest*. Ensemble learning method that uses multitude of decision trees.
LMT. Logistic Model Tree		

Table 4. ANOVA table for the experimental measurements.

Parameter	Degree of Freedom	Sum of Squares	Mean Square	F-Ratio	p-Value
f	2	7312.79	3656.40	142.31	$1.09 \cdot 10^{-48}$
d	1	134.15	134.15	5.22	0.023
w	1	95.47	95.47	3.72	0.054
v	1	183.08	183.08	7.13	0.008
h	1	3725.76	3725.76	145.01	$3.62 \cdot 10^{-29}$
θ	9	23862.50	2651.38	103.20	$7.73 \cdot 10^{-104}$
Error	453	11638.60	25.6922		
Total	468	46952.30			

Table 5. Classification algorithms' performance metrics.

Algorithm	Correctly Classified Instances	Incorrectly Classified Instances	Kappa Statistic
NaiveBayes	80.25	19.75	0.4919
LibVSM	62.63	37.37	0.114
Logistic	75.79	24.21	0.4219
MLP (NN)	91.51	8.49	0.8057
SMO	73.46	25.54	0.3982
IBk	93.20	6.80	0.8424
KStar	94.26	5.74	0.8668
Random Forest	95.11	4.89	0.8873
J48 (C4.5)	94.69	5.31	0.8771
LMT	94.69	5.31	0.8784

Table 6. Regression algorithms' performance metrics.

Algorithm	*r*	MAE / μm	RMSE / μm
Linear Regression	0.449	7.213	9.000
MLP	0.809	4.568	6.122
SMOreg	0.375	6.895	9.433
IBk	0.886	2.557	4.798
kStar	0.876	4.054	5.720
M5P	0.924	2.722	3.990
Random Forest	0.941	2.026	3.409

Caption to figures

Figure 1. Samples printed to different process parameter combinations.

Figure 2. Samples' surfaces obtained via a confocal microscope for different *f*, *h*, and θ.

Figure 3. Photographs of samples' surfaces obtained using a confocal microscope. PETG (a); PETG 12 (b); PETG 20 (c).

Figure 4. R_a measurements through different θ, for different *f* and *h*.

Figure 5. Main effect plots of studied factors on R_a.

Figure 6. Degree 2x4 polynomial R_a prediction model for different layer heights: *h*=0.1 mm (a) and *h*=0.2 mm (b).

Figure 7. J48 (C4.5) decision tree for five parameters: *h*, *f*, *d*, *s* and θ.

Figure 8. Random Forest predictions vs. actual R_a measures.

Figure 9. Actual sample: measures and estimations. Printed conditions: PTEG 20, *d* = 0.6 mm, *h* = 0.1 mm, *s* = 30 mm/s.

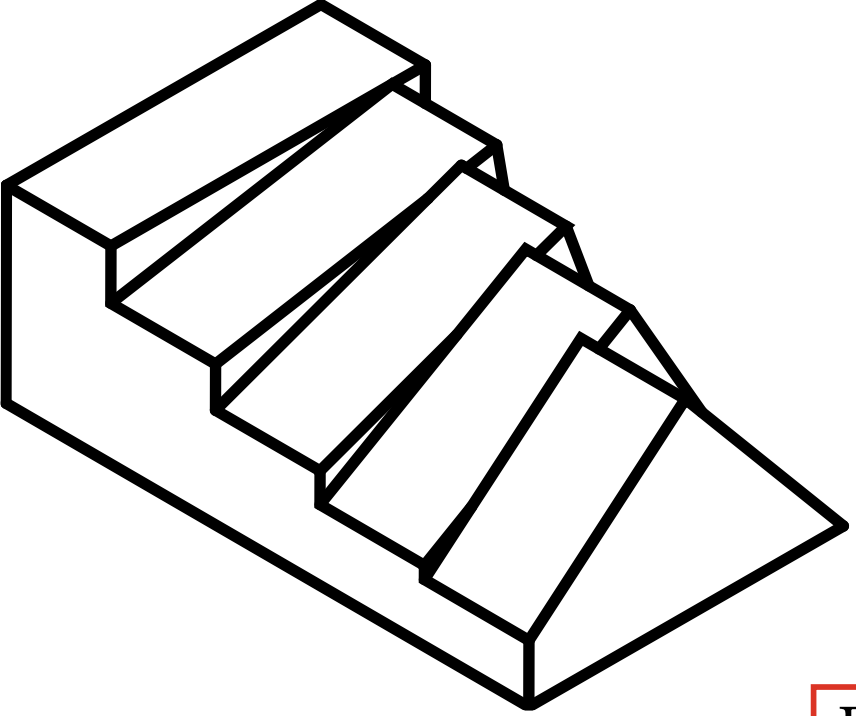

Samples

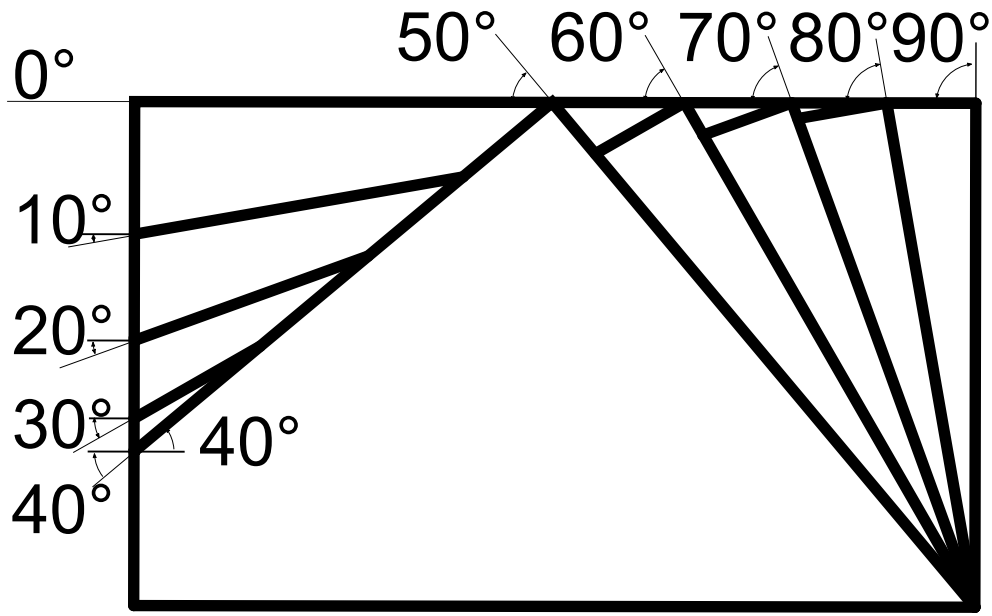

Surface build angle Θ

Figure 1

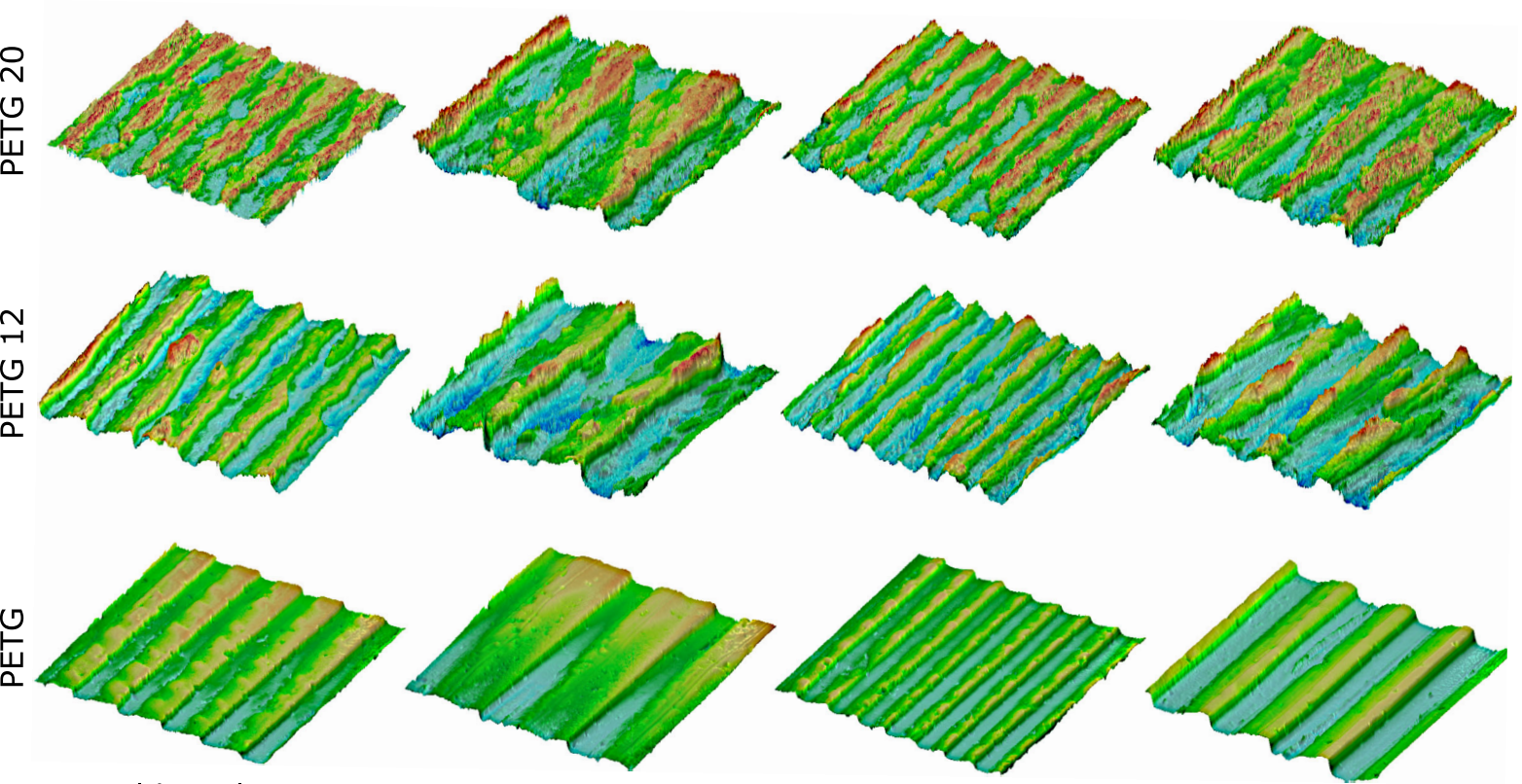
PETG 20
PETG 12
PETG
Z[µm]
185
160
135
110
95
70
45
0
Build Angle: 20º
h: 0.1mm
Buid Angle: 20º
h: 0.2mm
Build Angle: 30º
h: 0.1mm
Build Angle: 30º
h: 0.2mm

Figure 2

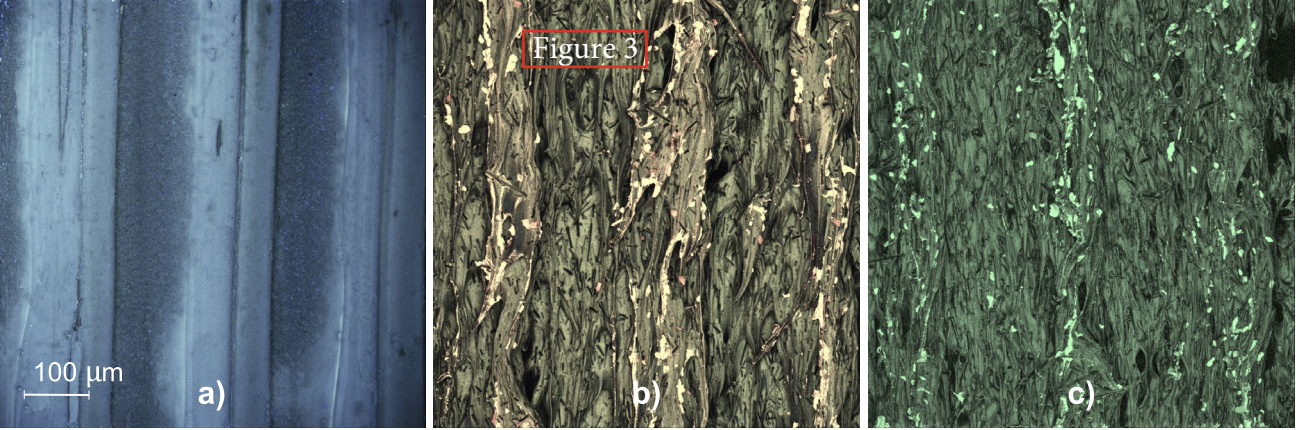
Figure 3
100 µm
a)
b)
c)

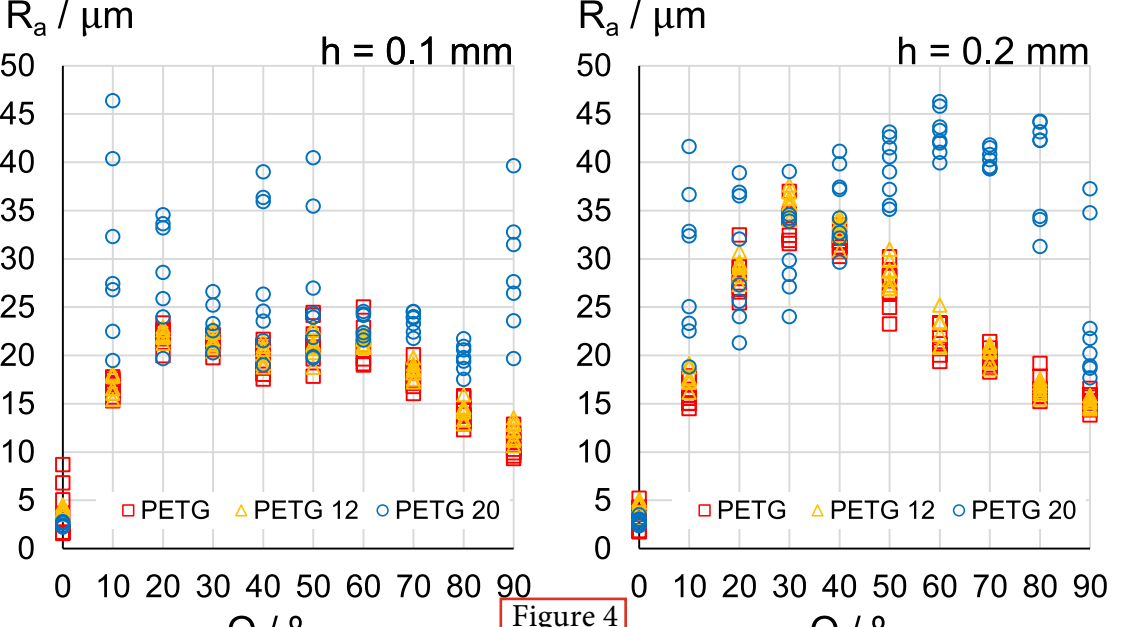
Ra / µm
h = 0.1 mm
50
45
40
35
30
25
20
15
10
5
0
PETG
PETG 12
PETG 20
0 10 20 30 40 50 60 70 80 90
Θ / °
Ra / µm
h = 0.2 mm
50
45
40
35
30
25
20
15
10
5
0
PETG
PETG 12
PETG 20
0 10 20 30 40 50 60 70 80 90
Θ / °

Figure 4

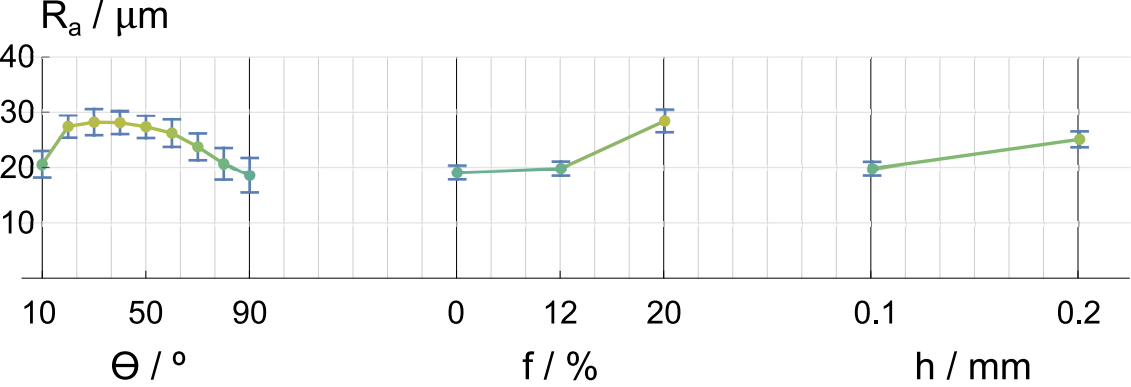
R_a / µm
40
30
20
10
10
50
90
Θ / °
0
12
20
f / %
0.1
0.2
h / mm

Figure 5

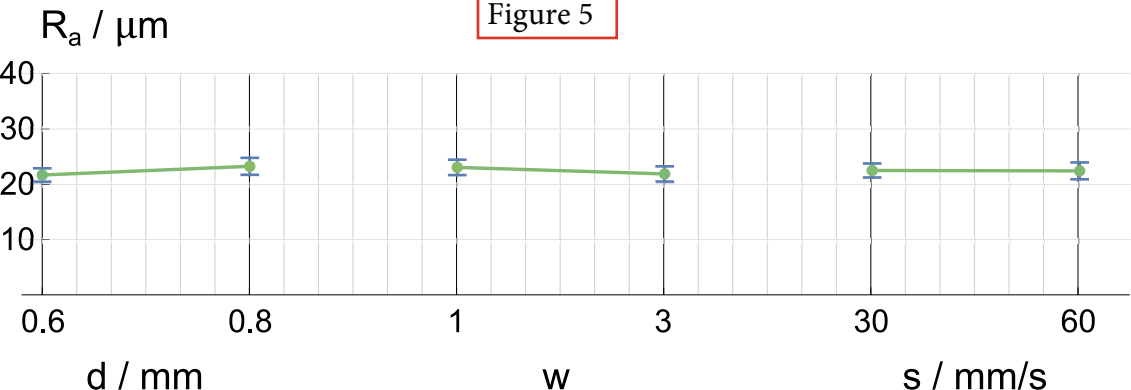
R_a / µm
40
30
20
10
0.6
0.8
d / mm
1
3
w
30
60
s / mm/s

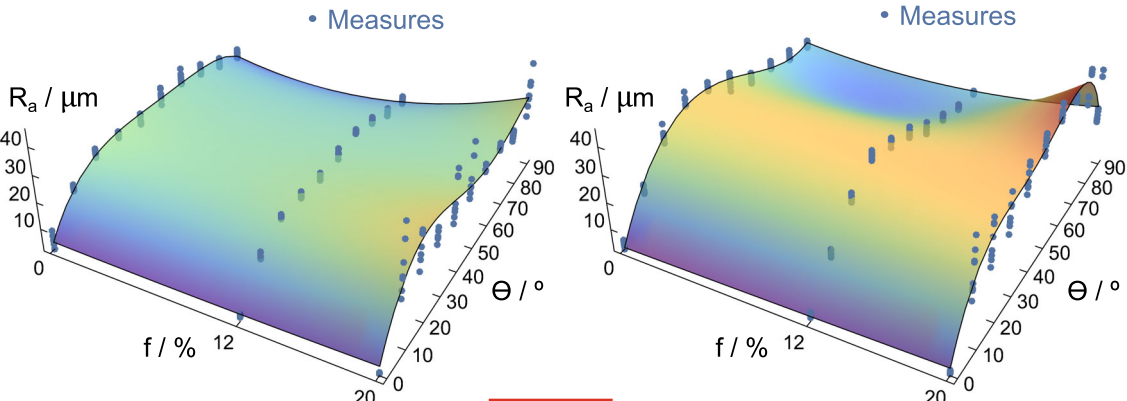

a) h = 0.1 mm

Figure 6

b) h = 0.2 mm

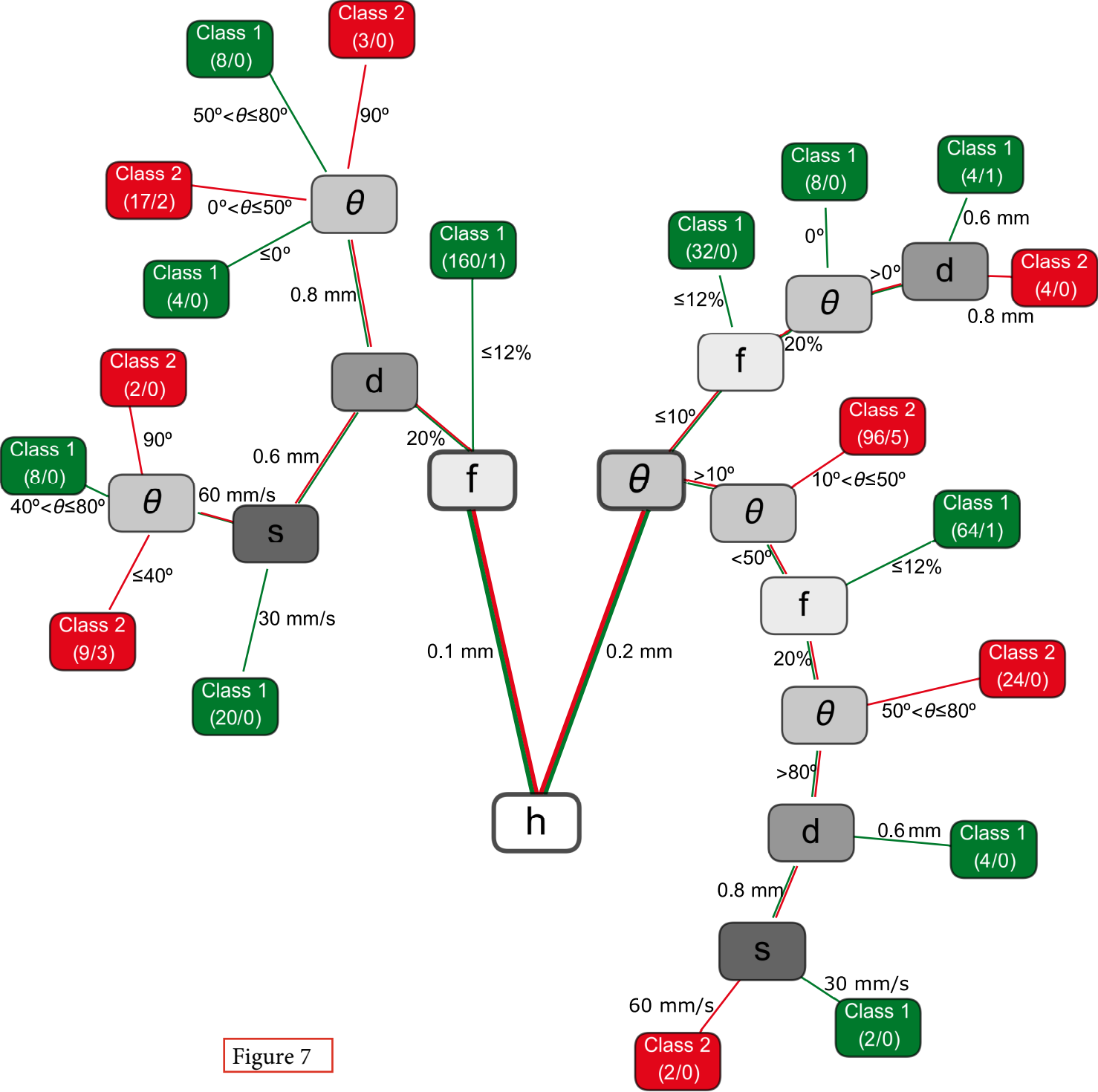
Class 1 (8/0)
Class 2 (3/0)
50°<θ≤80°
90°
Class 2 (17/2)
0°<θ≤50°
θ
≤0°
Class 1 (4/0)
0.8 mm
Class 1 (160/1)
≤12%
d
Class 2 (2/0)
90°
0.6 mm
20%
Class 1 (8/0)
40°<θ≤80°
θ
60 mm/s
s
f
≤40°
Class 2 (9/3)
30 mm/s
Class 1 (20/0)
0.1 mm
0.2 mm
h
Class 1 (8/0)
Class 1 (4/1)
0°
0.6 mm
Class 1 (32/0)
>0°
d
Class 2 (4/0)
≤12%
θ
0.8 mm
20%
f
≤10°
Class 2 (96/5)
θ
>10°
10°<θ≤50°
θ
Class 1 (64/1)
<50°
≤12%
f
20%
Class 2 (24/0)
θ
50°<θ≤80°
>80°
d
0.6 mm
Class 1 (4/0)
0.8 mm
s
30 mm/s
60 mm/s
Class 1 (2/0)
Class 2 (2/0)

Figure 7

Figure 8

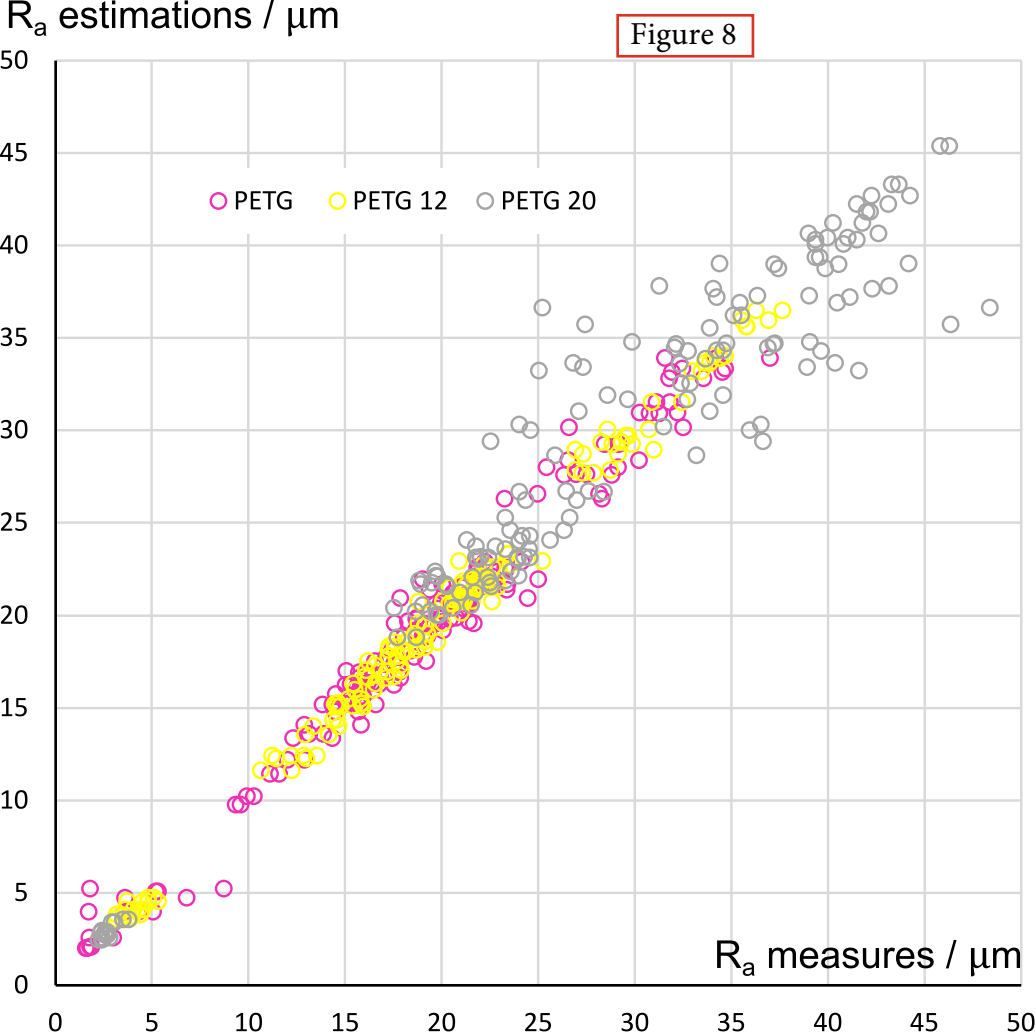
Ra estimations / µm
PETG
PETG 12
PETG 20
Ra measures / µm
0
5
10
15
20
25
30
35
40
45
50

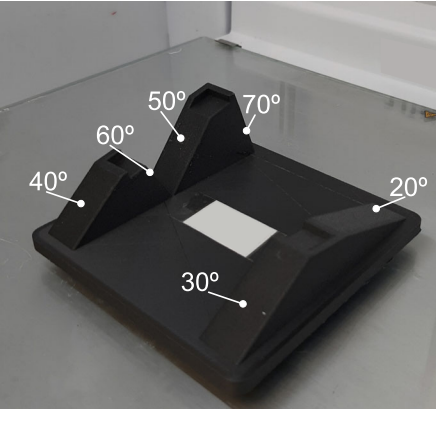
40º
60º
50º
70º
20º
30º

Figure 9

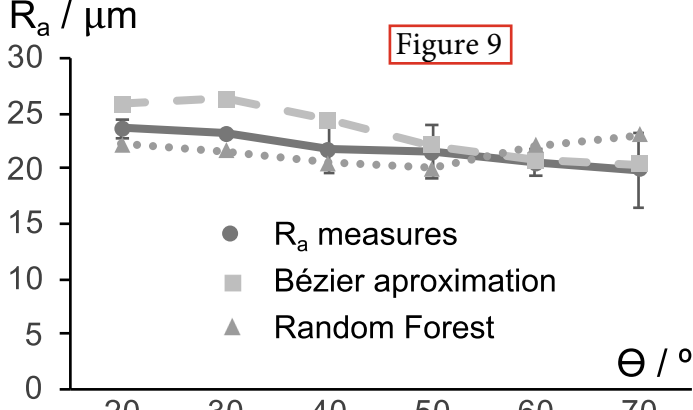
Ra / µm
30
25
20
15
10
5
0
Ra measures
Bézier aproximation
Random Forest
Θ / º
20
30
40
50
60
70